Sensors & Actuators: A. Physical 374 (2024) 115464

Contents lists available at ScienceDirect

Sensors and Actuators: A. Physical

journal homepage: www.journals.elsevier.com/sensors-and-actuators-a-physical

High-performance infrared photodetector based on InAs/GaAs submonolayer quantum dots grown at high temperature with a (2×4) surface reconstruction

A. Alzeidan [a,*], T.F. Cantalice [a], K.E. Sautter [b], K.D. Vallejo [b], P.J. Simmonds [b,c,d], A.A. Quivy [a]

[a] Institute of Physics, University of Sao Paulo, Sao Paulo, SP 05508-090, Brazil
[b] Micron School of Materials Science and Engineering, Boise State University, Boise, ID, USA
[c] Department of Physics, Boise State University, Boise, ID, USA
[d] Department of Electrical & Computer Engineering, Tufts University, Medford, MA, USA

ARTICLE INFO

Keywords:
Submonolayer quantum dot
Infrared photodetector
(2×4) surface reconstruction
2D-island nucleation
Indium segregation
Molecular beam epitaxy

ABSTRACT

We studied the impact of surface reconstruction on the performance of infrared photodetectors containing InAs/GaAs submonolayer quantum dots (SMLQDs) grown by molecular beam epitaxy. Adjusting the substrate temperature before InAs deposition allowed us to move between the conventional c(4×4) reconstruction of the GaAs (001) surface, observed at low growth temperatures, and the (2×4) reconstruction which can only be stabilized at higher sample temperatures than those commonly used to deposit InAs. Photodetectors based on SMLQDs grown on such a (2×4) surface reconstruction outperformed those grown on a c(4×4) reconstruction and provided specific detectivities as high as 8.3×10^{11} cm $Hz^{1/2}$ W^{-1} at 12 K. This increase in performance is due to the nucleation of true two-dimensional InAs islands which are the building blocks of SMLQDs and can only form on a (2×4)-reconstructed GaAs(001) surface.

1. Introduction

In recent years, semiconductor quantum dots (QDs) have attracted considerable attention due to interesting optoelectronic properties resulting from their three-dimensional (3D) carrier confinement. In addition, they exhibit completely discrete energy spectra similar to those of atoms [1–3], which is the reason why they are sometimes called artificial atoms. QDs have already been successfully used for device applications such as lasers [4,5], infrared photodetectors [6,7], and solar cells [8]. Due to these peculiar features, quantum-dot infrared photodetectors (QDIPs) have several benefits over the more popular quantum-well infrared photodetectors (QWIPs), including a lower dark current, normal-incidence detection, higher operating temperature, and higher detectivity [9–11].

Over the last three decades, most QDs used in solid-state samples and devices have been of the self-organized type obtained during deposition of InAs on a GaAs substrate in the Stranski-Krastanov growth mode [12,13]. While such nanostructures led to higher device performance compared to the use of quantum wells, some of their known drawbacks are limiting further improvement (low areal density, poor size control, presence of a wetting layer). QDs obtained with the submonolayer technique (SMLQDs) have recently been the subject of several studies. They offer some important advantages over conventional Stranski-Krastanov quantum dots (SKQDs), such as better size control, higher surface density, and the absence of a wetting layer [14–16]. InAs/GaAs SMLQDs are formed by depositing a fraction (typically 30 – 50 %) of a monolayer of InAs, followed by a few monolayers of GaAs, and then by repeating this process at will until the total desired amount of InAs has been deposited [17,18]. Ideally, the small two-dimensional (2D) InAs islands nucleated in consecutive InAs SMLs will align vertically—because of the local strain field originating from the lattice mismatch between both materials—to form columnar structures behaving as individual QDs. Due to the small lateral size of the original 2D InAs islands [15], SMLQDs have a larger height-to-base ratio than SKQDs. This increased lateral quantum confinement, together with the higher density of nanostructures, has resulted in QDIPs based on SMLQDs performing well under normal incidence illumination [19].

The molecular-beam-epitaxy (MBE) growth conditions for SMLQDs are more complex and their optimization is more challenging than those for conventional SKQDs, as they involve more experimental parameters.

* Corresponding author.
E-mail address: alzeidan@if.usp.br (A. Alzeidan).

https://doi.org/10.1016/j.sna.2024.115464
Received 18 March 2024; Received in revised form 8 May 2024; Accepted 10 May 2024
Available online 13 May 2024

This is perhaps the reason why almost all papers report InAs/GaAs SMLQDs grown under conditions similar to those for conventional SKQDs. These well-established growth conditions typically involve a substrate temperature around 480–515 °C and a high As flux (equivalent to 1.5–2.5 monolayers per second (ML/s)), leading unavoidably to the As-rich c(4×4) reconstruction of the GaAs(001) surface prior to InAs QD self-assembly. QDIPs containing SMLQDs grown under these conditions outperform devices based on SKQDs [20–22]. However, in-situ scanning tunneling microscopy (STM) studies have shown that the only way to form 2D InAs islands—the critical building blocks of SMLQDs—is to deposit the InAs material onto a GaAs(001) surface with an As-stabilized (2×4) surface reconstruction [23,24]. At a growth temperature of 490 °C, the (2×4) reconstruction can only be obtained by drastically reducing the As flux [25] down to 0.15–0.20 ML/s. Unfortunately, such a low As flux also reduces In incorporation [26] and increases In segregation [27], leading to layers with an overall lower In content and density of nanostructures [28] than when grown on a c(4×4) reconstructed surface.

There is, however, another way to stabilize the (2×4) reconstruction of the GaAs(001) surface. Instead of reducing the sample temperature from 570 °C (used to grow GaAs) to 490 °C (to deposit InAs)—which switches the reconstruction from the usual (2×4) pattern at high temperature to the c(4×4) pattern at some intermediate temperature (515–520 °C)—and then lowering the As flux to recover the original (2×4) pattern, as was previously done [29], one could lower the sample temperature to a value (525–530 °C) just slightly above that of the (2×4) to c(4×4) transition, in order to maintain the original (2×4) reconstruction. This higher growth temperature might slightly increase In segregation and desorption with respect to the other conditions previously used to reach the same surface reconstruction, but at least one could keep the As flux at a normal value, and In incorporation could recover its usual value.

In the present work, we grew, processed, and analyzed the performance of two QDIPs containing SMLQDs: one where InAs was deposited onto the conventional c(4×4) GaAs surface reconstruction, and another one where the InAs material was grown onto the (2×4) GaAs reconstruction obtained at a higher substrate temperature. We also compared their properties with those of a previous QDIP in the literature that had the same structure but contained SMLQDs grown on GaAs(001) with a (2×4) reconstruction obtained the other way, i.e., using a lower sample temperature and As flux.

2. Experimental details

The two QDIPs under consideration were grown by MBE on semi-insulating GaAs(001) substrates. Their structure consisted of two 1 μm-thick Si-doped GaAs layers ($n = 1\times10^{18}$ cm^{-3}) grown at 570 ℃, acting as bottom and top contacts. In between them, the active region was formed by ten GaAs quantum wells (QWs) containing the InAs SMLQDs, each surrounded by 45 nm-wide $Al_{0.1}Ga_{0.9}As$ barriers deposited at 580 °C (Fig. 1). The inner part of each of the QWs started with 1.3 nm of GaAs followed by the SMLQDs. The SMLQDs consisted of six repetitions of a basic cycle containing 0.5 ML of InAs, deposited at 0.1 ML/s, and a 2.5 ML GaAs spacer deposited at 1.0 ML/s. After the sixth cycle, 2.1 nm of GaAs were further grown. Each 2.5 ML-thick GaAs interlayer was Si-doped ($n = 2\times10^{18}$ cm^{-3}) to provide an adequate number of electrons to the SMLQDs. The As_2 flux was kept constant during the full growth and was equivalent to 1.90 ML/s. The only difference between both samples was the temperature at which the inner part of the QWs was deposited. After growing each $Al_{0.1}Ga_{0.9}As$ barrier at 580 °C, the substrate was cooled to 490 ℃ for sample A and to 525 ℃ for sample B. The inner part of the QW was deposited, and then the temperature was raised back to 580 °C to grow the next $Al_{0.1}Ga_{0.9}As$ barrier.

Reflection high-energy electron diffraction (RHEED) was used to calibrate the growth rates, identify both surface reconstructions, and determine the sample temperature at which the transition between the (2×4) and c(4×4) reconstructions occurred. Since this happened around 520 ℃ for the growth conditions described above, the SMLQDs of sample A were deposited on a c(4×4)-reconstructed surface, while those of sample B were grown on a (2×4) surface [25]. Although the (2×4) to c(4×4) transition could be observed along the [110] azimuthal direction commonly used for growth-rate calibration, the transition temperature was more accurately determined along the [010] direction,i.e., at 45° from the previous one. Indeed, the periodicity of the RHEED pattern is one-fold for the (2×4) surface and four-fold for the c(4×4) surface along [010], while it is two-fold for both reconstructions along [110] [25,29]. Since the substrate temperature of sample B was higher than usual for InAs deposition, the growth rate of that material was previously calibrated at the same temperature to take account of the slightly stronger In desorption in sample B and ensure an equal amount of InAs was deposited in both samples. The substrate temperature was monitored during growth using an infrared pyrometer and did not vary by more than ±2 ℃.

Both samples were processed into 400×400 μm^2 mesas using

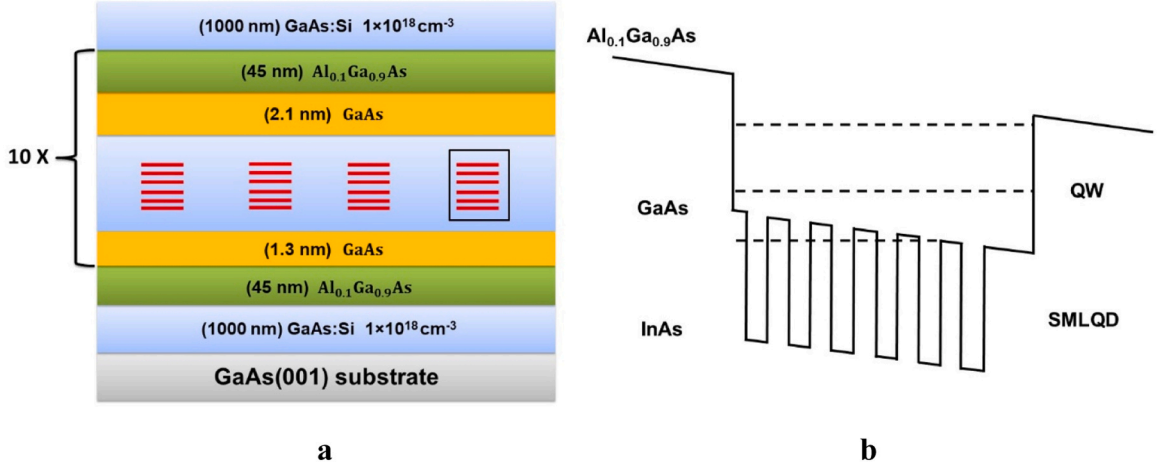

Fig. 1. a) Structure of samples A and B containing SMLQDs (black rectangle) formed by repeating six times a basic cycle consisting of 0.5 ML of InAs (red) followed by 2.5 MLs of GaAs. The SMLQDs of sample A were grown at 490 °C in the presence of a c(4×4) reconstruction of the GaAs(001) surface, while those of sample B were deposited at 525 °C with a (2×4) reconstruction. b) Conduction-band diagram of the nominal structure of the devices under bias. The dotted lines represent the energy levels of confined states.

standard optical lithography, wet etching, and electron-beam metallization. Rapid thermal annealing (520 °C for 30 s) was used to alloy the thin metallic layers (Ni/Ge/Au, 25/55/150 nm) and obtain good ohmic contacts. Then, the samples were fixed in a commercial chip carrier, and their mesas were wire bonded with thin Au wires to its conductive pads. Finally, the chip carrier was installed on the cold finger of a closed-cycle optical cryostat to check the optical and electrical properties of the devices between 12 and 300 K.

Three extra samples were also grown to perform photoluminescence (PL) measurements and assess more specifically the optical properties of SMLQDs. Sample C contained a single layer of SMLQDs similar to those of device A (c(4×4) reconstruction), while sample D had a single layer of SMLQDs as deposited in sample B ((2×4) reconstruction at high temperature and As flux), both without any doping. Sample E was similar to sample D, i.e., grown with a (2×4) reconstruction but at a lower temperature and As flux, as reported for an earlier device [29].

3. Results

The absorption spectrum of both SMLQDIPs was measured by Fourier transform infrared (FTIR) spectroscopy under normal incidence, i.e., with the radiation reaching the mesas from the top. Fig. 2 shows the results for samples A and B obtained at 12 K with a bias voltage of 1.8 V and 0.9 V, respectively. These specific biases were chosen, as they provide the maximum specific detectivity for each device, as will be shown later. The absorption spectrum of sample B is broader—the full width at half maximum (FWHM) is approximately 16.0 meV—and redshifted ($\lambda_{max} = 10.4$ μm) compared to sample A (FWHM ≈ 13.8 meV, $\lambda_{max} = 8.9$ μm). The redshift is caused by the stronger In surface segregation that occurs at higher substrate temperatures. Instead of incorporating into the SMLQDs, a fraction of the In atoms rides at the epi surface and part of it is evaporated later when the substrate is heated to grow the next $Al_{0.1}Ga_{0.9}As$ barrier. As a result, the SMLQDs grown at 525 °C contain slightly less In and hence have a wider band gap than those grown at 490 °C, despite the same amount of InAs being nominally deposited in both samples. The broader peak in sample B is probably also related to the enhanced In surface segregation that seems to induce a more inhomogeneous distribution of the size or composition of the SMLQDs.

The photocurrent of the SMLQDIPs was measured at 12 K in front of a calibrated black body set at 800 °C. The black-body responsivity of both devices was calculated by taking the ratio of the electrical output (photocurrent generated in the mesas) to the optical input (power of the infrared radiation falling on their optical area). Fig. 3 shows that the responsivity of sample B, grown in the presence of a (2×4) surface reconstruction at a higher temperature, is typically 10 times higher than that of the c(4×4) reference device (sample A) at the same bias voltage. Since the devices were processed simultaneously in the same way and have equal size, it means that, under similar experimental conditions, device B produces ten times more output signal than device A.

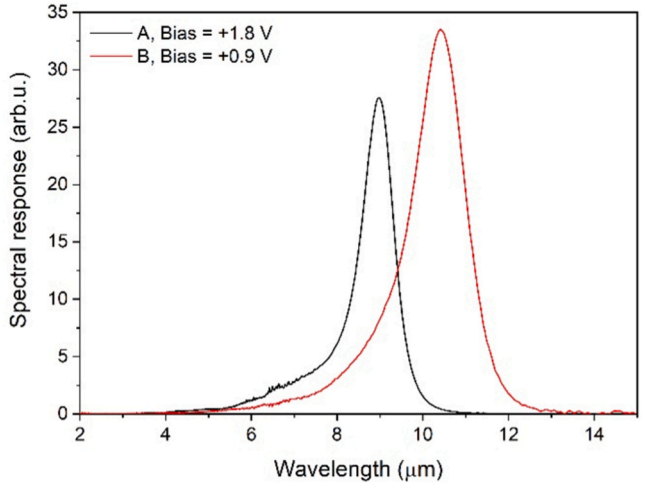

Fig. 2. Spectral response of SMLQDIPs A and B obtained by FTIR under normal incidence at 12 K with a bias voltage of 1.8 V and 0.9 V, respectively. These bias values are those where the detectivity of both devices is maximum.

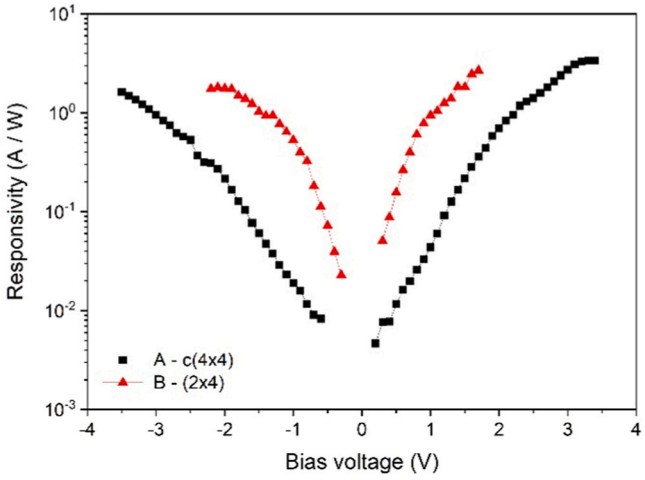

Fig. 3. Black-body responsivity of SMLQDIPs A and B under normal incidence as a function of bias at 12 K.

The photodetectors were then covered with a copper shield, allowing us to perform current-voltage (I×V) and noise measurements in the dark. As there was good thermal contact between the copper shield and the sample holder, the copper shield also acted as a cold shield. Fig. 4a shows that, for a given bias, the dark current of sample B is several orders of magnitude higher than that of sample A, which is consistent with the higher ground-state energy of those SMLQDs suggested by the redshift observed in Fig. 2. This leads to a smaller activation energy in sample B (57 meV) compared to sample A (91 meV), as calculated from an Arrhenius plot of temperature-dependent I×V measurements in the dark (Fig. 4b).

The noise-current spectral density was calculated by dividing the root-mean-square (RMS) noise current coming from the devices by the square root of the bandwidth of the noise spectrum used by the spectrum analyzer (Fig. 5). In general, the main noise source in a photoconductive photodetector is related to the generation-recombination (g-r) noise from the dark current. Thermal and Shot noise are usually much weaker, as is 1/f noise when the measurements are performed far from the low-frequency region [30]. It is therefore expected that the noise curves in Fig. 5 show the same trends as the dark-current curves in Fig. 4a. The plateau observed at low bias is due to the noise floor of the experimental setup that prevents any measurement below 4×10^{-14} A $Hz^{-1/2}$ [29].

The specific detectivity D^* is the major figure of merit of a detector as it allows a quantitative comparison of devices having different sizes or measured in different experimental conditions. It is related to the black-body responsivity (R) and noise current density (i_n) and is defined as $D^* = R\sqrt{A}/i_n$, where A is the optical area of the mesas [30]. Fig. 6 shows D^* as a function of bias voltage at 12 K for samples A and B. Although the responsivity is a monotonic function of bias (Fig. 3), the detectivity curves have a maximum due to the steep noise increase beyond a certain bias voltage (Fig. 5). Maximum specific detectivities of 3.7×10^{11} cm $Hz^{1/2}$ W^{-1} and 8.3×10^{11} cm $Hz^{1/2}$ W^{-1} were achieved in SMLQDIPs A and B at 1.8 and 0.9 V, respectively. Device B shows better performance because its noise floor is narrower than that of the control device, and the onset of its noise occurs at a bias (± 0.9 V) where the responsivity of the (2×4) device is much higher than that of the reference c(4×4) device. The detectivity of device B seems to be so far the highest ever reported for a SMLQDIP at helium temperature. However, it is worth

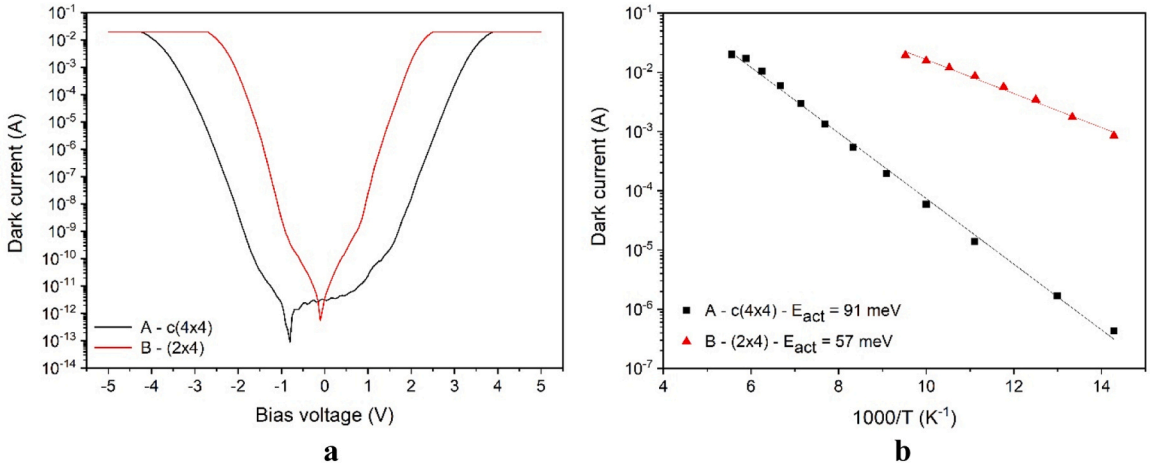

Fig. 4. a) Current versus voltage (I×V) curves in the dark (dark current) of SMLQDIPs A and B obtained at 12 K using a dark+cold shield. The current saturation at high bias is due to the compliance of the curve tracer that was set to 20 mA. b) Arrhenius plot of the dark current as a function of temperature to calculate the activation energy of the SMLQDs in devices A and B close to 0 V.

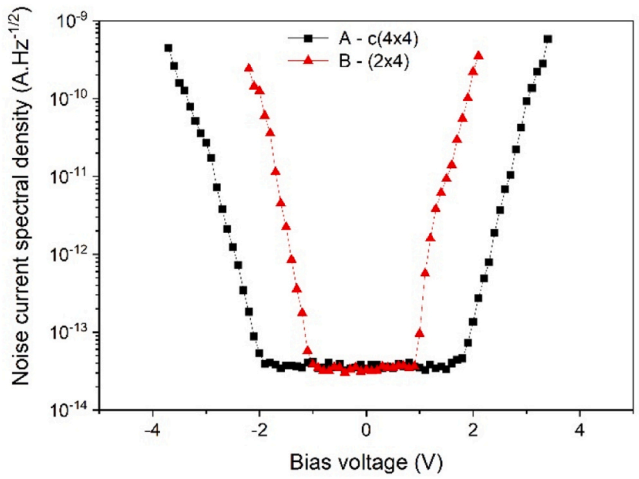

Fig. 5. Noise-current spectral density of SMLQDIPs A and B as a function of bias voltage at 12 K with a dark+cold shield.

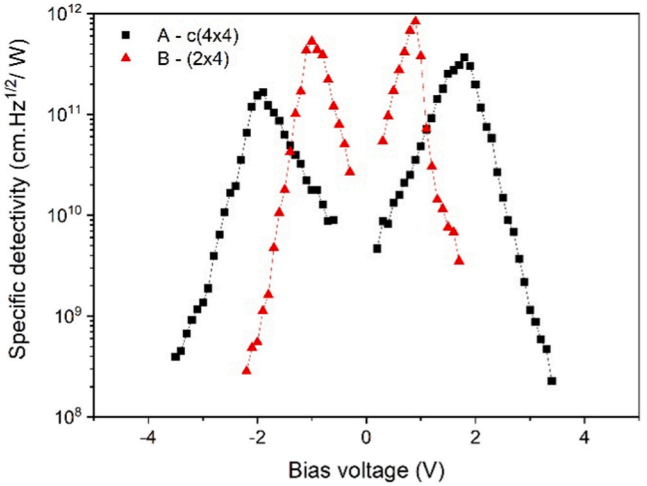

Fig. 6. Specific detectivity of SMLQDIPs A and B as a function of bias voltage at 12 K.

mentioning that slightly lower values were obtained at liquid-nitrogen temperature [20,31,32] and higher values were also reported [33] but for a device operating in the near-infrared using interband instead of intraband transitions (Table 1).

4. Discussion

Although, theoretically, SMLQDs seem to have many advantages over SKQDs—better control of the height of the structures, higher density, and absence of a wetting layer—in practice, things are different. Unlike SKQDs, which can be easily imaged by atomic force microscopy, the structural properties of SMLQDs are more difficult to assess as they are grown in a planar way and provide no relevant profile to be measured. The only technique that has been able so far to provide some useful information is cross-sectional scanning tunneling microscopy (XSTM), as it can provide atomically resolved images of buried structures and some clues about their size, geometry, and composition. XSTM measurements have already pointed out that the alternate deposition of a fraction of InAs monolayer during SMLQD growth doesn't actually lead to stacks of 2D InAs islands, as expected and often sketched (see Fig. 1). Instead, In-rich $In_xGa_{1-x}As$ clusters are observed, which are embedded in a thick In-poor $In_yGa_{1-y}As$ layer (x>y) [15,28]. These clusters are usually lower in height than expected and show no internal periodicity along the growth direction, suggesting that they are not columnar structures of 2D InAs islands. This is not very surprising, as most results in the literature are related to SMLQDs grown in conditions similar to those of SKQDs, i.e., low substrate temperature and high As flux. However, such conditions invariably lead to a c(4×4) reconstruction of the GaAs(001) surface that results in random incorporation of the In atoms and formation of a superficial InGaAs alloy instead of 2D InAs islands [23]. Nevertheless, it seems that the In-rich agglomerates

Table 1
Maximum specific detectivity (D*), operation temperature (T), wavelength (λ), type of structure, and publication year of InAs/GaAs SML-QD-based infrared photodetectors with a specific detectivity higher than 1.0×10^{11} cm $Hz^{1/2}$ W^{-1}.

D* (cm $Hz^{1/2}$ W^{-1})	T (K)	λ (μm)	Structure	year
8.3×10^{11}	12	12.4	Dot in a well [this work]	2024
4.2×10^{12}	80	0.88	Only QDs [33]	2019
3.2×10^{11}	77	6.05	Quantum Cascade [32]	2017
5.4×10^{11}	77	7.2	Dot in a well [31]	2014
1.2×10^{11}	77	7.5	Dot in a well + Confinement enhancing barriers [20]	2012

detected in the XSTM images of these samples do behave as QDs, and several types of devices containing SMLQDs grown in such conditions already perform better than with SKQDs [22,34]. Recently, Alzeidan and coworkers [29,35] attested the first QDIP containing SMLQDs grown in the presence of a (2×4) GaAs(001) reconstruction, which is the surface predicted to nucleate true 2D InAs islands [24]. However, they found that SMLQDIPs obtained with a c(4×4) and (2×4) surface reconstruction had similar performance. XSTM experiments revealed that, even in the presence of a (2×4) surface reconstruction, the nanostructures observed in the samples were irregular In-rich clusters with no periodicity and no evidence of 2D InAs islands [28]. However, the SMLQDs grown on the (2×4) surface were smaller, had a lower In content, and had an areal density ten times lower than that of SMLQDs grown on the usual c(4×4) reconstruction. The most meaningful explanation for both surface reconstructions leading to similar nanostructures was that In segregation, which is known to be very strong in the InAs/GaAs system, removes most In atoms from the 2D InAs islands on the (2×4) surface and spreads them to form the thick InGaAs layer observed around the In-rich clusters. When fitting the In-content profile of their XSTM images with the empirical model of Muraki et al. [26], Gajjela and coworkers [28] pointed out that, for the extreme growth conditions required to stabilize the (2×4) surface reconstruction prior to SMLQDs deposition—i.e., very low As flux (equivalent to 0.15 ML/s) and low InAs and GaAs growth rates (0.015 ML/s and 0.1 ML/s, respectively)—the In segregation coefficient R was larger than that obtained on a c(4×4) surface at higher As flux (R=0.83 vs. 0.72). That was confirmed by Cantalice et al. [27] on both types of surface reconstruction using the intensity decay of RHEED oscillations during deposition of InGaAs on top of GaAs(001) in similar growth conditions [36], [37]. As a consequence, most In atoms are removed from the original 2D InAs islands which, as a result, are no longer able to generate a strain field in the thin GaAs layers around them that is strong enough to align the 2D islands of the subsequent InAs submonolayers, as was already suggested by Alzeidan et al. [35]. This is why SMLQDs do not develop their full height, show no internal periodicity, and look like irregular In-rich clusters embedded in a thick InGaAs layer containing less In, even when grown on the (2×4) surface reconstruction.

Therefore, In segregation seems to be the main problem to solve in order to obtain SMLQDs closer to our expectations. If one could reduce the segregation coefficient, more In would remain in the original 2D islands and the strain field around them would be stronger, leading to better vertical stacking. Additionally, a higher In content would lower the band gap of the material and provide better confinement of the carriers. As segregation is thermally activated, the segregation coefficient R can be written as

$$R = R_0 \exp(E_a/kT) \quad (1)$$

where R_0 is a constant, E_a is the activation energy of the segregation process, k is Boltzmann's constant, and T is the absolute temperature of the sample during deposition. Thus, the easiest way to reduce the strength of In segregation would be to lower the substrate temperature. However, lower temperatures also result in a higher number of structural defects, so a compromise must be found. Moreover, the activation energy of In surface segregation in the InAs/GaAs system is only 0.11–0.12 eV [26,36], which means that temperature must be decreased by more than 200 °C if one wishes to lower R to half its original value, something that is difficult to reconcile with good crystalline quality.

Nevertheless, limiting In segregation is not the only way to keep the In content of the original 2D InAs islands at a higher level. Indeed, in their attempt to grow SMLQDs at a low temperature in the presence of a (2×4) surface reconstruction, Gajjela et al. [28] had to considerably decrease the As flux and observed in their XSTM images that the In content of their samples was lower than with a c(4×4) surface, because In incorporation was reduced at low As flux [26]. As a consequence, the In contents of the In-rich clusters and thick InGaAs layer around them were lower than on a c(4×4) surface, and so was the density of clusters which also had a smaller size. In the present work, we wished to avoid all the drawbacks related to using a low As flux to get a (2×4) surface reconstruction. We only cooled the substrate to 525 ºC under the usual high As flux, maintaining the original (2×4) reconstruction observed at high temperature and avoiding the transition to the c(4×4) reconstruction. Of course, the higher sample temperature (525 °C instead of 490 °C) will increase In segregation but, as will be shown below, it turned out that the benefits from the higher As flux outweigh the negative effects of the higher substrate temperature. When the segregation coefficient R_1 at a certain temperature T_1 is known, Eq. 1 provides the following relation to easily calculate R_2 at another temperature T_2, as long as all the other growth parameters are kept unchanged:

$$R_2 = R_1 \exp\left(\frac{-E_a}{k}\left(\frac{1}{T_2} - \frac{1}{T_1}\right)\right) \quad (2)$$

Using the activation energy mentioned above (0.11–0.12 eV) and the segregation coefficient R=0.83 obtained in the XSTM images of Gajjela et al. [28] for SMLQDs grown on a (2×4) surface at 490 °C, one could expect a value of R=0.90 at 525 °C (see Table 2), if the other growth conditions of our sample B were similar to those used in [28]. However, as the As flux and InAs and GaAs growth rates of sample B investigated here were kept at their normal values, i.e., much higher than in the samples investigated in [28], they contribute to lowering segregation [35]. Using Eq. 2, one can also estimate that, with the new growth conditions used in sample B—which are similar to those of the c(4×4) sample investigated in [27] except for its lower growth temperature of 515 °C—the In-segregation coefficient of sample B grown at 525 °C should be around 0.79 instead of 0.77 in [27]. As a consequence, although a higher substrate temperature of 525 °C was used in sample B to get a (2×4) surface, its segregation coefficient was lower (R=0.79) than that of the sample grown in a previous study (R=0.83 in [35]) with the same surface reconstruction but at a lower temperature (490 °C) and much lower As flux and growth rates. However, as a high As flux could be kept in sample B, In incorporation was also back to its normal value, which increased further the In content of the nanostructures. These features altogether are responsible for the superior properties of sample B observed in the figures of merit presented above that will now be analyzed in more detail.

XSTM images clearly show that the In-rich clusters that act as QDs—we will keep calling them SMLQDs for the sake of simplicity—are only a few nm wide and high [15,28]. As their nominal In content is

Table 2
Values of the In segregation coefficient R in SMLQDs grown in different conditions. The values with uncertainties were experimentally measured by XSTM [28] and RHEED [27]. The bold values without uncertainties were calculated from the experimental data using Eq. 2 and are used in the discussion. The other cells were kept empty for the sake of clarity but can also be calculated from Eq. 2. The R values of samples A and B were obtained from the sample grown at 515 °C using Eq. 2 and their respective temperature (the other growth parameters were the same).

Growth conditions of SMLQDs				Segregation coefficient R		
Reconstruction	**As flux**	**Growth rate**	**Ref/ sample**	**490 °C**	**515 °C**	**525 °C**
c(4×4)	High	Low	[28]	0.72 (2)		
(2×4)	Low	Low	[28]	0.83 (2)		**0.90**
c(4×4)	High	High	[27]	**0.73**	0.77 (1)	**0.79**
(2×4)	Low	Low	[27]	0.81 (2)		
c(4×4)	High	High	Sample A	**0.73**		
(2×4)	High	High	Sample B			**0.79**

originally low (only 33 % in the case of samples A and B investigated here), their material has quite a large band gap, and the nanostructures have only a single confined state which corresponds to their ground state [38]. Fig. 2 shows that their absorption spectrum is narrow—$\Delta\lambda/\lambda$ is equal to 0.09 and 0.14 for samples A and B, respectively—suggesting that the transition occurs between two confined states (bound-to-bound transition), i.e., from the ground state of the SMLQDs to the first (and only) excited state of the AlGaAs/GaAs quantum well, where they can escape from to the continuum through the AlGaAs barriers by field-effect tunneling (Fig. 1b). Although samples A and B have exactly the same structure and the same (nominal) In fraction in their SMLQDs, the absorption of sample B grown at 525 °C is redshifted. Its In segregation coefficient (R=0.79) is higher than that of sample A (R=0.73) obtained with the same growth conditions but at 490 °C and, consequently, with a c(4×4) reconstruction. Hence, the In content of the SMLQDs is lower in sample B than in sample A, leading to a material with a larger gap and a shift of their ground state toward higher energies. This results in a lower transition energy to the excited state of the AlGaAs/GaAs quantum well and in a redshift of the absorption spectrum of sample B, as seen in Fig. 2. The stronger segregation of sample B also means that more In atoms are randomly removed from the original 2D InAs islands. The lower their In content, the stronger the effect that any small variation of composition or size will have on the energy of the SMLQD ground state, leading thus to a broader absorption peak in sample B.

The superior performance of device B obtained with a (2×4) surface reconstruction seems to be mainly due to its 10-fold higher responsivity, as seen in Fig. 3. It may result from a higher population of the ground state of the SMLQDs or a more effective extraction of the photoexcited carriers from the excited state of the AlGaAs/GaAs quantum well. The last possibility can be easily ruled out as those quantum wells were grown in the same conditions in both devices, and their excited levels should be identical. This is not the case for the first possibility that was raised, as, although the doping of the SMLQDs themselves was identical in both devices, the SMLQDs were grown at very different temperatures (490 °C and 525 °C in devices A and B, respectively). It is well known that InAs and GaAs are best grown at 500–515 °C and 570–580 °C, respectively. Growing both materials at 490 °C, as in sample A, introduces more structural defects that worsen the optical and transport properties of the epitaxial layers. Defects can generate deep levels that can trap carriers from the original dopant atoms or open non-radiative recombination channels, reducing the net amount of carriers available for populating the ground state of the SMLQDs and participating in the photoexcitation process. Growing the SMLQDs at 525 °C, as in sample B, reduces the density of defects and contributes to improving device performance. The Si doping used in the present study was originally experimentally calibrated for SMLQDs grown at 490 °C in the conditions of sample A and was kept the same in sample B [35] to avoid changing more than one parameter at a time. As sample B was grown at a higher temperature, there are fewer defects and more carriers are probably available to take part in the absorption process, yielding its increased performance. Additionally, as the segregation coefficient is higher in sample B, more 2D InAs islands might be fully dissolved, which would reduce the final density of SMLQDs and contribute to increasing the availability of carriers as well. However, one can see in Fig. 4 that the dark current of sample B is also much higher than in the other device, which could result from an excess of carriers that might raise the Fermi level of the SMLQDs and provide a lower activation energy. Consequently, an optimization (most probably a reduction) of the doping for the new growth conditions of sample B could lower the dark current—and consequently the noise in the device that is taken into account in the calculation of the detectivity—and provide a device with even better performance.

Fig. 7 shows the photoluminescence (PL) spectra of samples C and D that contain each only a single layer of SMLQDs similar to those present in devices A and B, respectively. The wavelength ranges of Figs. 2 and 7

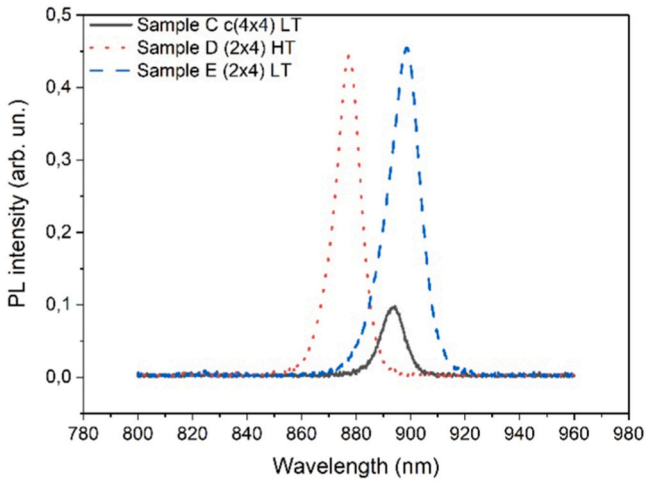

Fig. 7. PL spectra of samples C and D which contain a single layer of SMLQDs grown in the same conditions as those of devices A and B, respectively. Sample E is used for comparison and contains a single layer of SMLQDs grown in the presence of a (2×4) surface reconstruction at low temperature (LT) and low As flux, as in ref [28]. Sample D was the only one grown at higher temperature (HT). All the measurements were performed at 77 K.

are very different, as the emission spectra of Fig. 7 involve transitions across the band gap of the nanostructures, while the absorption spectra of Fig. 2 are related to transitions inside the conduction band. Because the average In content of SMLQDs is much lower (nominally 33 % In for these specific SMLQDs instead of 100 % In for SKQDs), they emit at shorter wavelengths than SKQDs whose PL spectra usually peak around 1000 nm. One can also see in Fig. 7 that both emissions are quite narrow—16.4 meV and 17.4 meV for samples C and D, respectively—and much narrower than that of conventional InAs SKQDs which commonly have a full width at half maximum (FWHM) around 60–80 meV [39]. Although this is often intuitively attributed to a higher homogeneity of the size distribution of SMLQDs when compared to SKQDs, this is obviously not the case, as already observed in XSTM images of SMLQDs which reveal a huge variety of sizes and shapes [15,16,28]. Using magneto-optical measurements, Harrison et al. showed that this narrow emission was actually resulting from the small size of SMLQDs—which appear as $In_xGa_{1-x}As$ clusters embedded in a wider $In_yGa_{1-y}As$ layer (with x>y)—leading to the confinement of holes in individual SMLQDs, while the wave function of electrons was only weakly localized and was able to overlap simultaneously several nanostructures and the $In_yGa_{1-y}As$ matrix around them [16]. As a consequence, the PL spectrum of InAs/GaAs SMLQDs is more similar to that of an InGaAs/GaAs QW—due to the leakage of the electrons' wave function into the thick $In_yGa_{1-y}As$ layer around them—than to the PL spectrum of an ensemble of conventional InAs/GaAs SKQDs. However, a layer of SMLQDs must definitely not be considered as a QW. For instance, the extremely high detectivity observed in Fig. 6 is incompatible with a QW, as electronic intraband transitions are forbidden in 2D systems (QWs) when radiation impinges under normal incidence on their surface, as is the case here. The high performance of the devices investigated in this work is undeniably related to the presence of 3D confinement in the In-rich clusters and cannot be attributed to any interface roughness or alloy fluctuations that are typically observed in QWs. It was actually shown that the larger the difference in Indium content between the In-rich clusters and the surrounding InGaAs matrix, the stronger the confinement of both electrons and holes in the SMLQDs [16,34].

The difference in Indium content between the In-rich clusters and the InGaAs layer around them is actually at the origin of the higher PL intensity of sample D, which is no coincidence and was also reported for SMLQDs grown in the presence of the (2×4) surface reconstruction obtained at lower temperature and much lower As pressure [34,38].

Indeed, in this last case, XSTM images suggested that, although the average In content in the SMLQDs layers was lower than that detected with the c(4×4) reconstruction, the difference in content between the In-rich clusters and the surrounding InGaAs matrix was larger [28]. Therefore, electrons and holes are more effectively confined, the overlap of their wave functions is stronger, and, consequently, the PL emission is expected to be more intense [34]. This is confirmed in Fig. 7 where sample E—which has exactly the same structure as sample C but was grown in the presence of a (2×4) surface reconstruction stabilized at low temperature and As flux, as in [28]—exhibits a PL emission much stronger than that of sample C. The same reasoning applies to samples C and D: although segregation is stronger in sample D (0.79 vs. 0.73), the fact that real 2D InAs islands are only nucleated on the (2×4)-reconstructed GaAs(001) surface favors the formation of In-rich clusters with, comparatively, more In than in the InGaAs layer around them, leading to the higher PL intensity. Since sample D, that was grown at 525 °C with a (2×4) reconstruction, and sample E, that was also grown with a (2×4) reconstruction but at 490 °C, have a similar PL intensity—which is several times higher than that of sample C—it means that the enhanced intensity of sample D is probably not due to its improved crystalline quality (resulting from the higher growth temperature) but rather to the larger difference in Indium content between the In-rich clusters and the surrounding InGaAs layer, as was the case in sample E. The blueshift observed in sample D with respect to sample E suggests that this effect might even be stronger in sample D. Indeed, since its segregation coefficient is smaller (0.79 vs. 0.83) and the In incorporation is back to its usual value due to the higher As flux, the band gap of the clusters must be lower than in sample E, the clusters are most probably larger, and therefore both effects should lead to a redshift instead of a blueshift. As a consequence, one possible explanation would be an increase of strain in the clusters, resulting from an increase in the difference in Indium content between them and the surrounding InGaAs layer [40].

5. Conclusion

InAs/GaAs SMLQDs are usually grown on a GaAs(001) surface with a c(4×4) reconstruction, using the same well-established growth conditions as for InAs/GaAs SKQDs. However, it seems that a (2×4) reconstruction is required to nucleate the 2D InAs islands that must stack vertically to provide good SMLQDs. During a recent attempt in this direction, the very low As flux required to recover the (2×4) reconstruction at the low substrate temperatures commonly used to deposit InAs resulted in reduced incorporation of the In atoms and a lower density of smaller SMLQDs than with the c(4×4) reconstruction. Here, we instead used a higher sample temperature to maintain the original (2×4) reconstruction just above its transition to the c(4×4) reconstruction. In such conditions, the As flux and growth rates could be kept at their normal values and In incorporation came back to its expected level, which were the two main drawbacks for growing SMLQDs on the (2×4) reconstruction using the previous conditions. An infrared photodetector containing SMLQDs grown with these new parameters (device B) showed a record specific detectivity of 8.3×10^{11} cm $Hz^{1/2}$ W^{-1} at 12 K for a wavelength of 10.4 μm, which is several times larger than that of similar devices grown in conventional conditions with a c(4×4) reconstruction (device A) or even with a (2×4) reconstruction obtained at lower temperature and As flux. This superior performance seems to originate from the improved nucleation and conservation of true 2D InAs islands that can only form on the (2×4) surface. However, In segregation is very strong in the InAs/GaAs system and scatters most In atoms (70–80 %) in the surrounding layers, leading to In-rich $In_xGa_{1-x}As$ clusters embedded in a thick $In_yGa_{1-y}As$ layer (x>y). Although In segregation is stronger in sample B than in sample A—due to its higher growth temperature—the initial presence of true 2D InAs islands in sample B provides In-rich InGaAs clusters that contain more In than their surroundings, comparatively to sample A, which improves 3D carrier confinement. The new growth conditions investigated here are much easier and faster to reach than those proposed earlier for the same surface reconstruction and provide better results. Additionally, the high dark current detected in device B seems to be related to doping in excess of the SMLQDs, suggesting that further optimization could yield devices with even higher performance.

CRediT authorship contribution statement

A. Alzeidan: Writing – original draft, Visualization, Validation, Investigation, Formal analysis, Data curation. **T.F. Cantalice:** Investigation. **K.E. Sautter:** Investigation. **K.D. Vallejo:** Investigation. **P.J. Simmonds:** Writing – review & editing, Supervision, Resources, Funding acquisition. **A.A. Quivy:** Writing – review & editing, Supervision, Resources, Project administration, Methodology, Funding acquisition, Conceptualization.

Declaration of Competing Interest

The authors declare that they have no known competing financial interests or personal relationships that could have appeared to influence the work reported in this paper.

Data Availability

Data will be made available on request.

Acknowledgements

This study was financed in part by the Coordenação de Aperfeiçoamento de Pessoal de Nível Superior - Brasil (CAPES) - Finance Code 001, and by CNPq (grant 309837/2021–9).

References

[1] L. Goldstein, F. Glas, J.Y. Marzin, M.N. Charasse, G. LeRoux, Growth by molecular beam epitaxy and characterization of InAs/GaAs strained-layer superlattices, Appl. Phys. Lett. 47 (1985) 1099, https://doi.org/10.1063/1.96342.
[2] S. Farad, R. Leon, D. Leonard, J.L. Merz, P.M. Petroff, Phonons and radiative recombination in self-assembled quantum dots, Phys. Rev. B 52 (1995) 5752, https://doi.org/10.1103/PhysRevB.52.5752.
[3] L. Chu, M. Arzberger, G. Bohm, G. Abstreiter, Influence of growth conditions on the photoluminescence of self-assembled InAs/GaAs quantum dots, J. Appl. Phys. 85 (1999) 2355, https://doi.org/10.1063/1.369549.
[4] Q. Xie, A. Kalburge, P. Chen, A. Madhukar, Observation of lasing from vertically self-organized InAs three-dimensional island quantum boxes on GaAs (001), IEEE Photonics Technol. Lett. 8 (1996) 965–967, https://doi.org/10.1109/68.508705.
[5] Z. Yao, C. Jiang, X. Wang, H. Chen, H. Wang, L. Qin, Ziyang Zhang, Recent developments of quantum dot materials for high speed and ultrafast lasers, Nanomaterials 12 (2022) 1058, https://doi.org/10.3390/nano12071058.
[6] S.D. Gunapala, D.R. Rhiger, C. Jagadish, Advances in Infrared Photodetectors, Semiconductors and Semimetalsvol., Elsevier, 2011. ISBN 978-01-2381-337-4.
[7] P. Martyniuk, S. Krishna, A. Rogalski, Assessment of quantum dot infrared photodetectors for high temperature operation, J. Appl. Phys. 104 (2008) 034314, https://doi.org/10.1063/1.2968128.
[8] C.G. Bailey, D.V. Forbes, R.P. Raffaelle, S.M. Hubbard, Near 1 V open circuit voltage InAs/GaAs quantum dot solar cells, Appl. Phys. Lett. 98 (2011) 163105, https://doi.org/10.1063/1.3580765.
[9] J. Phillips, Evaluation of the fundamental properties of quantum dot infrared detectors, J. Appl. Phys. 91 (2002) 4590–4594, https://doi.org/10.1063/1.1455130.
[10] V. Ryzhii, I. Khmyrova, M. Ryzhii, V. Mitin, Comparison of dark current responsivity and detectivity in different intersubband infrared photodetectors, Semicond. Sci. Technol. 19 (2003) 8–16, https://doi.org/10.1088/0268-1242/19/1/002.
[11] S. Krishna, Quantum dots-in-a-well infrared photodetectors, J. Phys. D 38 (2005) 2142–2150, https://doi.org/10.1088/0022-3727/38/13/010.
[12] S. Guha, A. Madhukar, K.C. Rajkumar, Onset of incoherency and defect introduction in the initial stages of molecular beam epitaxical growth of highly strained InxGa1−xAs on GaAs(100), Appl. Phys. Lett. 57 (1990) 2110–2112, https://doi.org/10.1063/1.103914.
[13] D. Leonard, M. Krishnamurthy, C.M. Reaves, S.P. Denbaars, P.M. Petroff, Direct formation of quantum-sized dots from uniform coherent islands of InGaAs on GaAs surfaces, Appl. Phys. Lett. 63 (1993) 3203–3205, https://doi.org/10.1063/1.110199.
[14] I.L. Krestnikov, N.N. Ledentsov, A. Hoffmann, D. Bimberg, Arrays of two-dimensional islands formed by submonolayer insertions: growth, properties,

devices, Phys. Stat. Sol. (a) 183 (2001) 207–233, https://doi.org/10.1002/1521-396X(200102)183:2<207::AID-PSSA207>3.0.CO;2-2.
[15] A. Lenz, H. Eisele, J. Becker, J.-H. Schulze, T.D. Germann, F. Luckert, K. Pötschke, E. Lenz, L. Ivanova, A. Strittmatter, D. Bimberg, U.W. Pohl, M. Dähne, Atomic structure and optical properties of InAs submonolayer depositions in GaAs, J. Vac. Sci. Technol. B 29 (2011) 04D104, https://doi.org/10.1116/1.3602470.
[16] S. Harrison, M.P. Young, P.D. Hodgson, R.J. Young, M. Hayne, L. Danos, A. Schliwa, A. Strittmatter, A. Lenz, H. Eisele, U.W. Pohl, D. Bimberg, Heterodimensional charge-carrier confinement in stacked submonolayer InAs in GaAs, Phys. Rev. B 93 (2016) 085302, https://doi.org/10.1103/PhysRevB.93.085302.
[17] J.O. Kim, S. Sengupta, A.V. Barve, Y.D. Sharma, S. Adhikary, S.J. Lee, S.K. Noh, M. S. Allen, J.W. Allen, S. Chakrabarti, S. Krishna, Multi-stack InAs/InGaAs sub-monolayer quantum dots infrared photodetectors, Appl. Phys. Lett. 102 (2013) 011131, https://doi.org/10.1063/1.4774383.
[18] S. Sengupta, A. Mandal, H. Ghadi, S. Chakrabarti, K.L. Mathur, Comprehensive study on molecular beam epitaxy-grown InAs sub-monolayer quantum dots with different capping combinations, J. Vac. Sci. Technol. B 31 (2013) 03C136, https://doi.org/10.1116/1.4805018.
[19] J.O. Kim, Z. Ku, A. Urbas, S.J. Lee, Investigation of the shape of submonolayer quantum dots using a polarization-dependent photocurrent, Semicond. Sci. Technol. 30 (2015) 115005, https://doi.org/10.1088/0268-1242/30/11/115005.
[20] S. Sengupta, J.O. Kim, A.V. Barve, S. Adhikary, Y.D. Sharma, N. Gautam, S.J. Lee, S.K. Noh, S. Chakrabarti, S. Krishna, Sub-monolayer quantum dots in confinement enhanced dots-in-a-well heterostructure, Appl. Phys. Lett. 100 (2012) 191111, https://doi.org/10.1063/1.4711214.
[21] D.Z.-Y. Ting, Y.-C. Chang, B. Rafol, J.K. Liu, C.J. Hill, S.A. Keo, J. Mumolo, S. D. Gunapala, S.V. Bandara, The sub-monolayer quantum dot infrared photodetector revisited, Infrared Phys. Technol. 70 (2015) 20–24, https://doi.org/10.1016/j.infrared.2014.09.028.
[22] H. Ghadi, S. Sengupta, S. Shetty, A. Manohar, A. Balgarkashi, S. Chakrabarti, N. B. Pendyala, S.L. Prajapati, A. Kumar, Comparison of three design architectures for quantum dot infrared photodetectors: InGaAs-capped dots, dots-in-a-well, and submonolayer quantum dots, IEEE Trans. Nanotechnol. 14 (2015) 603, https://doi.org/10.1109/TNANO.2015.2432044.
[23] J.G. Belk, C.F. McConville, J.L. Sudijono, T.S. Jones, B.A. Joyce, Surface alloying at InAs-GaAs interfaces grown on (001) surfaces by molecular beam epitaxy, Surf. Sci. 387 (1997) 213–226, https://doi.org/10.1016/S0039-6028(97)00355-5.
[24] G.R. Bell, T.J. Krzyzewski, P.B. Joyce, T.S. Jones, Island size scaling for submonolayer growth of InAs on GaAs(001)-(2×4): strain and surface reconstruction effects, Phys. Rev. B 61 (2000) R10551, https://doi.org/10.1103/PhysRevB.61.R10551.
[25] V.P. LaBella, M.R. Krause, Z. Ding, P.M. Thibado, Arsenic-rich GaAs(001) surface structure, Surf. Sci. Rep. 60 (2005) 1–53, https://doi.org/10.1016/j.surfrep.2005.10.001.
[26] K. Muraki, S. Fukatsu, Y. Shiraki, R. Ito, Surface segregation of In atoms during molecular beam epitaxy and its influence on the energy levels in InGaAs/GaAs quantum wells, Appl. Phys. Lett. 61 (1992) 557–559, https://doi.org/10.1063/1, 107835.
[27] T.F. Cantalice, A. Alzeidan, S.M. Urahata, A.A. Quivy, In-situ measurement of Indium segregation in InAs/GaAs submonolayer quantum dots, Mater. Res. Express 6 (2019) 126205, https://doi.org/10.1088/2053-1591/ab55a8.
[28] R.S.R. Gajjela, A.L. Hendriks, A. Alzeidan, T.F. Cantalice, A.A. Quivy, P. M. Koenraad, Cross-sectional scanning tunneling microscopy of InAs/GaAs(001) submonolayer quantum dots, Phys. Rev. Mater. 4 (2020) 114601, https://doi.org/10.1103/PhysRevMaterials.4.114601.
[29] A. Alzeidan, M.S. Claro, A.A. Quivy, High-detectivity infrared photodetector based on InAs submonolayer quantum dots grown on GaAs(001) with a 2 × 4 surface reconstruction, J. Appl. Phys. 126 (2019) 224506, https://doi.org/10.1063/1.5125238.
[30] J.D. Vincent, Fundamentals of Infrared Detector Operation and Testing, Wiley, 1990. ISBN 0-471-50272-3.
[31] J.O. Kim, Z. Ku, A. Kazemi, A. Urbas, S.-W. Kang, S.K. Noh, S.J. Lee, S. Krishna, Effect of barrier on the performance of sub-monolayer quantum dot infrared photodetectors, Opt. Mater. Express 4 (2014) 198, https://doi.org/10.1364/OME.4.000198.
[32] J. Huang, D. Guo, W. Chen, Z. Deng, Y. Bai, T. Wu, Y. Chen, H. Liu, J. Wu, B. Chen, Sub-monolayer quantum dot quantum cascade mid -infrared photodetector, Appl. Phys. Lett. 111 (2017) 251104, https://doi.org/10.1063/1.5011239.
[33] S. Mukherjee, S. Mukherjee, A. Pradhan, T. Maitra, S. Sengupta, S. Chakrabarti, A. Nayak, S. Bhunia, Carrier transport and recombination dynamics of InAs/GaAs sub-monolayer quantum dot near infrared photodetector, J. Phys. D Appl. Phys. 52 (2019) 505107, https://doi.org/10.1088/1361-6463/ab414b.
[34] T. Borrely, A. Alzeidan, M.D. de Lima, G.M. Jacobsen, T.-Y. Huang, Y.-C. Yang, T. F. Cantalice, R.S. Goldman, M.D. Teodoro, A.A. Quivy, Viability of intermediate band solar cells based on InAs/GaAs submonolayer quantum dots and the role of surface reconstruction, Sol. Energy Mater. Sol. Cells 254 (2023) 112281, https://doi.org/10.1016/j.solmat.2023.112281.
[35] A. Alzeidan, T.F. Cantalice, K.D. Vallejo, R.S.R. Gajjela, A.L. Hendriks, P. J. Simmonds, P.M. Koenraad, A.A. Quivy, Effect of As flux on InAs submonolayer quantum dot formation for infrared photodetectors, Sens. Actuators A Phys. 334 (2022) 113357, https://doi.org/10.1016/j.sna.2021.113357.
[36] S. Martini, A.A. Quivy, E.C.F. da Silva, J.R. Leite, Real-time determination of the segregation strength of indium atoms in InGaAs layers grown by molecular-beam epitaxy, Appl. Phys. Lett. 81 (2002) 2863, https://doi.org/10.1063/1.1513182.
[37] S. Martini, A.A. Quivy, T.E. Lamas, M.J. da Silva, E.C.F. da Silva, J.R. Leite, Influence of indium segregation on the RHEED oscillations during the growth of InGaAs layers on a GaAs(0 0 1) surface, J. Cryst. Growth 251 (2003) 101–105, https://doi.org/10.1016/S0022-0248(02)02313-8.
[38] T.F. Cantalice, A. Alzeidan, G.M. Jacobsen, T. Borrely, M.D. Teodoro, A.A. Quivy, Evidence of weak strain field in InAs/GaAs submonolayer quantum dots, Micro Nanostruct. 172 (2022) 207449, https://doi.org/10.1016/j.micrna.2022.207449.
[39] J.G. Keizer, A.B. Henriques, A.D.B. Maia, A.A. Quivy, P.M. Koenraad, Atomically resolved study of the morphology change of InAs/GaAs quantum dot layers induced by rapid thermal annealing, Appl. Phys. Lett. 101 (2012) 243113, https://doi.org/10.1063/1.4770371.
[40] K. Nishi, H. Saito, S. Sugou, J.-S. Lee, A narrow photoluminescence linewidth of 21 meV at 1.35 μm from strain-reduced InAs quantum dots covered by In0.2Ga0.8As grown on GaAs substrates, Appl. Phys. Lett. 74 (1999) 1111–1113, https://doi.org/10.1063/1.123459.

A. Alzeidan obtained a Bachelor of Science degree in Physics from the University of Damascus (Syria) in 2011, and a Masterś degree (2017) and Ph.D. (2023) in Physics from the University of São Paulo (Brazil). His expertise is related to the growth of III–V heterostructures by molecular beam epitaxy and the optimization, processing, and testing of infrared photodetectors based on InAs/GaAs submonolayer quantum dots.

T.F. Cantalice obtained a Bachelor of Science degree in Physics from the State University of São Paulo (Brazil) in 2012, a Master's degree in Physics from the State University of Campinas (Brazil) in 2015, and a Ph.D. in Physics from the University of São Paulo (Brazil) in 2023. His expertise is related to the investigation of indium segregation and strain in infrared photodetectors based on InAs/GaAs quantum dots. He is also currently working as a Data Scientist for a British independent provider of commodity price information company.

K.E. Sautter is a Sr. R&D molecular beam epitaxy engineer at IQE in North Carolina. She completed her Bachelor of Science in materials science and engineering at Penn State in 2017, and received her Ph.D. in materials science and engineering from Boise State University in spring 2021. Her Ph.D. work consisted of investigating tensile-strained III-V and IV quantum dots grown by molecular beam epitaxy (MBE). She then moved onto a post-doctoral position at Argonne National Laboratory to work on the epitaxy of rare earth oxide materials for quantum memory applications. In fall 2022, she began a career at IQE.

K.D. Vallejo is a staff scientist at the Idaho National Laboratory (INL). He obtained a B.S. degree in Physics from the University of Texas at El Paso in 2016, a M.Engr. degree and a Ph.D. in Materials Science and Engineering from Boise State University in 2020 and 2021, respectively. Kevin has received the U.S. Department of State's Benjamin A. Gilman scholarship, the U.S. National Nuclear Science Foundation Graduate Fellowship, and the U.S. Intelligence Community Postdoctoral Fellowship. Kevin currently runs the first molecular beam epitaxy laboratory at INL where he and his team study novel nitride materials ranging from transition metals to actinides.

P.J. Simmonds completed his Ph.D. in semiconductor physics at the University of Cambridge in 2008, followed by postdoctoral positions at the University of Minnesota, UCSB, Yale, and UCLA, where he chaired the IEEE Photonics Society chapter. From 2014–2023, Dr. Simmonds was a faculty member in Physics and Materials Science at Boise State University. He is now Associate Professor in Electrical & Computer Engineering at Tufts University with interests in electronic, photonic, and quantum materials. He is a Senior Member of the IEEE, winner of the 2018 North American Molecular Beam Epitaxy Young Investigator award, and a US National Science Foundation CAREER awardee.

A.A. Quivy graduated in 1986 and got his Masterś degree (1986) and Ph.D. (1991) in Physics from Université Libre de Bruxelles (Belgium). He has been a Professor of Physics at Universidade de São Paulo (Brazil) since 1992, was a visiting scientist at the Center for Quantum Devices (Northwestern University, USA) in 2005 and 2006, and is an Associate Professor since 2012. His main research topics are molecular beam epitaxy and morphological, structural, and opto-electrical characterization of III–V compounds. Lately, he has been investigating the growth, processing and testing of III–V solar cells and infrared photodetectors based on quantum dots.